

# Demodulation and Tracking With Dirty Templates for UWB Impulse Radio: Algorithms and Performance

Shahrokh Farahmand, Xiliang Luo, *Student Member, IEEE*, and Georgios B. Giannakis, *Fellow, IEEE*

(Invited Paper)

**Abstract**—Major challenges in ultrawideband (UWB) communications include timing acquisition, tracking, and low complexity demodulation. Timing with dirty templates (TDT) is a recently proposed acquisition algorithm with attractive features. Starting with a performance analysis of TDT, this paper goes on to considerably broaden its scope by developing novel tracking loops and detectors by naturally following the TDT operation. Specifically, upper bounds on the mean square error of the blind and data-aided TDT estimators are derived, along with TDT-based demodulators, obviating the need to know the underlying channel and time hopping code. Analytical comparisons reveal that TDT demodulators outperform RAKE with limited number of fingers in the medium-high SNR range. TDT demodulation performance in the presence of timing errors is evaluated and shown to be robust to mistiming. In order to follow timing offset variations, an adaptive loop is also introduced to track the first multipath arrival of each symbol. For a given input disturbance, parameters of the loop are selected to optimize jointly transient and steady state performance. Analytical results are corroborated by simulations.

**Index Terms**—RAKE receiver, synchronization, time lock loops, timing offset estimation, tracking performance, ultra-wideband (UWB).

## I. INTRODUCTION

ULTRAWIDEBAND (UWB) impulse radio (IR) offers great potential in terms of low power, enhanced user capacity, high data rates and ability to coexist with legacy services. Most of these benefits originate from the unique characteristics inherent to UWB wireless transmissions [22]. However, to harness these benefits, UWB-IR faces several challenges, among which low-complexity timing and demodulation are particularly critical. Timing UWB transmissions is more complicated than usual because the ultrashort information bearing pulses place stringent constraints on acquisition and tracking, which compromise demodulation performance when limited energy is captured.

Manuscript received February 19, 2005; revised June 1, 2005. The review of this paper was coordinated by Prof. X. Shen. This work was supported through collaborative participation in the Communications and Networks Consortium sponsored by the U.S. Army Research Laboratory under the Collaborative Technology Alliance Program, Cooperative Agreement DAAD19-01-2-0011. The U.S. Government is authorized to reproduce and distribute reprints for Government purposes notwithstanding any copyright notation thereon. This work is also supported by the NSF-ITR Grant No. EIA-0324864. Part of the results in this paper were submitted to *GLOBECOM Conf.*, St. Louis, MO, Nov. 28–Dec. 2, 2005; and *ICU Conf.*, Zurich, Switzerland, Sept. 5–8, 2005.

The authors are with the Department of Electrical and Computer Engineering, University of Minnesota, 200 Union Street, Minneapolis, MN 55455, USA. (e-mail: shahrokh@ece.umn.edu; xlluo@ece.umn.edu; georgios@ece.umn.edu).  
Digital Object Identifier 10.1109/TVT.2005.854032

Several timing algorithms have been proposed recently for UWB-IR. Maximum-likelihood (ML) [11] and least squares approaches [1] are available, but tend to be computationally complex as they require high sampling rates. Based on the cyclic mean of the received waveform, which is nonzero for pulse position modulation (PPM), blind timing and channel estimation schemes with lower complexity were put forth in [19]. A low complexity joint timing and template recovery algorithm for both PPM and PAM was proposed in [13] and [12], with universal applicability to UWB-IR in the presence or absence of intersymbol interference and multiuser interference. Timing with dirty templates (TDT), which is the starting point of this paper, was introduced in [23] for acquisition purposes; see also [18] and [22].

Regarding demodulation, RAKE was the first receiver considered for UWB-IR communications. But for its complexity and cost to remain low, the number of fingers that can be afforded is too small to capture the ample energy provided by the UWB channel, which entails a large number of paths (often >50). In addition, estimating tap gains and delays to form the RAKE template is costly and introduces errors which affect RAKE performance [16], [17]. An alternative to RAKE, is the so called transmitted reference (TR) receiver [5] and its optimized version known as pilot waveform assisted modulation (PWAM) [24], where a segment of the received waveform serves as a template for demodulation [25]. Comparisons between RAKE and TR can be found in [3], [21]. Similar to RAKE, TR and PWAM receivers require accurate timing synchronization as well as training to recover the reference template, which reduces bandwidth efficiency. This is mitigated in a recent low complexity approach where timing is acquired blindly and demodulation is based on what is termed synchronized aggregate template (SAT) [13]. This is the basis of the demodulator we pursue here, which relies on data-aided or blind TDT to acquire the timing information needed to form the SAT, which in turn effects reliable demodulation because it collects the full multipath energy provided by the UWB channel. Our performance comparisons will reveal that this is the main reason why TDT-based demodulation outperforms practical RAKE receivers that entail a limited number of fingers (typically <10).

To alleviate the effects of transmitter-receiver motion and oscillator drifts, time tracking loops are often employed to adaptively follow timing offset variations in the received waveform. Time lock loops (TLL) and phase locked loops (PLL) have been investigated extensively [4], [10], [14], [15], but not as thoroughly in the context of UWB-IR radios. A tracker following the

first received path in a cluster of multiple paths was designed and the effect of other multipath components on loop performance was considered in [2]. In this study, we combine TLL with TDT-based acquisition and demodulation, which enables tracking the symbol starting time instead of the first path in a cluster (which might not be the first cluster for that transmitted symbol).

The rest of this paper is organized as follows. Section II describes our system and outlines the TDT acquisition algorithm of [23]. In Section III, upper bounds on the mean square error of TDT estimators are derived. Section IV develops the novel TDT-based demodulator, analyzes its performance and compares it with the RAKE. A decision directed TLL is derived in Section V, where its performance is also analyzed in terms of output noise variance. For a known input, loop parameters are selected to optimize both transient and steady state performance. Corroborating simulations are provided in Section VI, and conclusions are drawn in Section VII.

## II. SYSTEM MODEL AND THE TDT ALGORITHM

For UWB-IR transmissions equipped with symbol periodic (a.k.a. short) time hopping (TH) codes, the transmitted waveform can be expressed as [20]

$$s(t) = \sqrt{\mathcal{E}_p} \sum_n s(n) p_T(t - nT_s)$$

$$p_T(t) := \sum_{m=0}^{N_f-1} p(t - mT_f - c_m T_c) \quad (1)$$

where  $\mathcal{E}_p$  is the energy per pulse,  $\{s(n) = \pm 1\}$  denotes binary PAM symbols, and  $p_T(t)$  is the symbol waveform of duration  $T_s = N_f T_f$  consisting of  $N_f$  frames, each of duration  $T_f$ . Each frame contains an ultrashort monocycle  $p(t)$  of duration  $T_p$  (in the order of ns), the position of which is shifted by the user-specific TH code  $c_m$  entailing  $N_c$  chips of duration  $T_c$ , per frame; i.e.,  $T_f = N_c T_c$  and  $\{c_m\}_{m=0}^{N_f-1} \in [0, N_c - 1]$ .

The UWB channel is modeled as a tapped delay line with real impulse response:  $h(t) = \sum_{l=0}^L \alpha_l \delta(t - \tau_{l,0} - \tau_0)$ , where  $\tau_0$  is the first path arrival time, and  $\tau_{l,0}$  is the arrival time of path  $l$  relative to path 0. Path gains  $\{\alpha_l\}_{l=0}^L$  and delays  $\{\tau_{l,0}\}_{l=0}^L$  are assumed invariant over a block of symbols (block fading model). The received waveform  $r(t)$  is then the convolution  $s(t) \star h(t)$  in the presence of multiuser interference (MUI)  $\rho(t)$  and additive Gaussian noise  $\eta(t)$  with double-sided power spectrum density  $\sigma^2/2$  and bandwidth  $B$  ( $\approx 1/T_p$ ) dictated by the cutoff frequency of the frontend ideal lowpass filter; i.e.,  $r(t) = h(t) \star s(t) + \eta(t) + \rho(t)$ , or

$$r(t) = \sqrt{\mathcal{E}_p} \sum_n s(n) p_R(t - nT_s - \tau_0) + \eta(t) + \rho(t) \quad (2)$$

where  $p_R(t) := p_T(t) \star h(t + \tau_0) = \sum_{m=0}^{N_f-1} \sum_{l=0}^L \alpha_l p(t - mT_f - c_m T_c - \tau_{l,0})$  is the aggregate received symbol waveform which accounts for the transmit filter, the channel, and the receiver's frontend filter. Given  $r(t)$ , our goal is to acquire  $\tau_0$ , track it, and demodulate to obtain an estimate  $\hat{s}(n)$  of  $s(n)$ . We further wish to analyze the performance of the  $\hat{\tau}_0$

and  $\hat{s}(n)$  estimators and compare the latter with the standard UWB-RAKE receiver.

To this end, we adopt the following operating conditions.

- 1) C1. Inter-symbol interference (ISI) is absent, but inter-frame interference and interpulse interference are allowed to be present. ISI can be avoided by selecting  $c_0, c_{N_f-1}$  and  $T_f$  to satisfy:  $c_{N_f-1} T_c + T_p + \tau_{L,0} < T_f + c_0 T_c$ ; or, by inserting zero guard frames of length  $\geq \tau_{L,0}$  at the end of each symbol. Either way, the aggregate received waveform  $p_R(t)$  has nonzero support  $[0, T_s]$ .
- 2) C2. In the data-aided (DA) mode with training symbols known at the receiver, if multiple users are present, only one is synchronized at a time; i.e., only one user sends the training sequence while others are allowed to communicate zero-mean information bearing symbols.

Based on C1 and C2, our results build on the TDT acquisition algorithm derived in [23] for DA and non-DA (a.k.a. blind) operation. DA-TDT relies on the training sequence  $\{s(n) = (-1)^{\lfloor n/2 \rfloor}\}$ , where  $\lfloor \cdot \rfloor$  denotes integer floor operation. The received waveform is then averaged over  $K$  consecutive segments of duration  $2T_s$  each. This yields a circularly shifted (by the wanted timing offset) demodulation template which, along with its periodic extension, are given by

$$\bar{r}(t) := \frac{1}{K} \sum_{k=0}^{K-1} (-1)^k r(t + 2kT_s), \quad t \in [0, 2T_s]$$

$$\tilde{r}(t) := (-1)^m \bar{r}((t)_{\text{mod } 2T_s}) \quad (3)$$

where  $m = (t - (t)_{\text{mod } 2T_s}) / (2T_s)$ . Although three DA-TDT variants have been derived in [23], we summarize next the one with best performance.

- 3) DA-TDT [23]: Under C1, C2, and with training pattern  $\{s(n) = (-1)^{\lfloor n/2 \rfloor}\}$ , timing offset  $\tau_0$  can be estimated using

$$\hat{\tau}_0 = \arg \max_{\tau \in [0, T_s]} J_{\text{DA}}(\tau)$$

$$J_{\text{DA}}(\tau) = \left( \int_{\tau}^{T_s + \tau} \tilde{r}(t) \tilde{r}(t + T_s) dt \right)^2 \quad (4)$$

The blind counterpart of (4) can be summarized as follows:

- 4) Non-DA TDT [23]: If MUI is absent, then timing offset  $\tau_0$  can be estimated blindly under C1 as

$$\hat{\tau}_0 = \arg \max_{\tau \in [0, T_s]} J_{\text{NDA}}(\tau),$$

$$J_{\text{NDA}}(\tau) = \frac{1}{K} \sum_{k=0}^{K-1} \left( \int_{2kT_s + \tau}^{(2k+1)T_s + \tau} r(t) r(t + T_s) dt \right)^2 \quad (5)$$

The basic idea behind TDT is to locate the maximum of the square of the correlation between pairs of successive symbol long segments of  $\tilde{r}(t)$  (in DA-TDT), or  $r(t)$  (in blind TDT). These symbol long segments are called "dirty templates" because: i) they are noisy, ii) they are distorted by the unknown channel, and iii) they are subject to the unknown offset  $\tau_0$ .

Notice that in addition to the channel, the TH code can be unknown. DA-TDT enjoys fast acquisition, while blind TDT incurs no rate loss.

Regarding implementation, the symbol long segments can be computed using either digital or analog operations. Analog approaches avoid the possibly high sampling rates needed in the UWB regime, but implementing the analog delay required to shift successive  $r(t)$  segments by  $T_s$  or  $2T_s$  can be challenging. Nonetheless, chips implementing analog delays from 20–1 000 ns are available [6]. On the other hand, when sampling at 1–2 GHz can be afforded, it is possible to store  $r(t)$  digitally, which facilitates the maximization required to find  $\hat{\tau}_0$ . As far as the maximization algorithm itself, we certainly need to evaluate  $J_{\text{DA}}$  or  $J_{\text{NDA}}$  over a finite grid of equispaced candidate offset values  $\tau$ . Spacing of these values depends on the desirable resolution which is constrained only by the affordable complexity: i) coarse timing with low complexity, e.g., by picking the maximum over  $N_f$  candidate offsets  $\tau_k = kT_f$ , where integer  $k \in [0, N_f)$ ; or ii) fine timing with higher complexity at the chip resolution with  $\tau_i = iT_c$ ,  $i \in [0, N_f N_c)$ .

Based on these TDT acquisition algorithms derived in [23], we will develop novel TDT-based demodulators and tracking loops. But first, we will analyze  $\hat{\tau}_0$  in (4) and (5) by deriving upper bounds on their mean square error (MSE), which will allow us to assess their asymptotic performance as  $K \rightarrow \infty$ .

### III. ASYMPTOTIC ANALYSIS OF TDT ESTIMATORS

Because  $J_{\text{NDA}}(\tau)$  and  $J_{\text{DA}}(\tau)$  are nonlinear functions of  $\tau$ , a general MSE analysis of  $\hat{\tau}_0$  is complicated, which typically prompts one to assess performance of TDT-based acquisition via simulations. However, when the signal-to-noise-ratio (SNR) is relatively high or the averaging size  $K$  is sufficiently large, it is possible to derive analytical upper bounds on the MSE of TDT estimators. We will derive such bounds, first for data-aided TDT.

#### A. DA-TDT

If the number of users contributing to  $\rho(t)$  in (2) is large, then the MUI will be approximately Gaussian (by virtue of the central limit theorem), and  $\rho(t)$  obeying C2 can be lumped into the AGN  $\eta(t)$ . We assume throughout this section that  $\tau_0 \in [0, T_s)$ , which we show in Appendix I incurs no loss of generality. With the training sequence  $\{s(n) = (-1)^{\lfloor n/2 \rfloor}\}$ , the sample average in (3) can be written for  $t \in [0, 2T_s]$  as (see Appendix I for a detailed derivation)

$$\begin{aligned} \bar{r}(t) &= \sqrt{\mathcal{E}_p} p_R(t - \tau_0) + \sqrt{\mathcal{E}_p} p_R(t - T_s - \tau_0) \\ &\quad - \sqrt{\mathcal{E}_p} p_R(t + T_s - \tau_0) + \bar{\eta}(t) \\ &:= \bar{r}_s(t) + \bar{\eta}(t), \quad t \in [0, 2T_s] \end{aligned} \quad (6)$$

where  $\bar{r}_s(t) := \sqrt{\mathcal{E}_p} p_R(t - \tau_0) + \sqrt{\mathcal{E}_p} p_R(t - T_s - \tau_0) - \sqrt{\mathcal{E}_p} p_R(t + T_s - \tau_0)$  and  $\bar{\eta}(t) := (1/K) \sum_{k=0}^{K-1} (-1)^k \eta(t + 2kT_s)$  are the noise-free and noisy parts of  $\bar{r}(t)$ , respectively. It can be readily shown that the variance of  $\bar{\eta}(t)$  is

$\text{Var}(\bar{\eta}(t)) = B\sigma^2/K$ . Using (6), we can rewrite  $J_{\text{DA}}(\tau)$  in (3) as

$$\begin{aligned} J_{\text{DA}}(\tau) &= \left[ \int_{\tau}^{T_s+\tau} \bar{r}_s(t) \bar{r}_s(t - T_s) dt + \int_{\tau}^{T_s+\tau} \bar{r}_s(t - T_s) \bar{\eta}(t) dt \right. \\ &\quad \left. + \int_{\tau}^{T_s+\tau} \bar{r}_s(t) \bar{\eta}(t - T_s) dt + \int_{\tau}^{T_s+\tau} \bar{\eta}(t - T_s) \bar{\eta}(t) dt \right]^2 \\ &:= [\chi(\tau) + \zeta(\tau)]^2 \end{aligned} \quad (7)$$

where  $\chi(\tau) := \int_{\tau}^{T_s+\tau} \bar{r}_s(t) \bar{r}_s(t - T_s) dt$  and  $\zeta(\tau)$  captures zero-mean noise-related terms. Several useful expressions for  $\zeta(\tau)$  are summarized below. They can be easily verified (see Appendix II).

$$\begin{aligned} E[\zeta^2(\tau)] &= \frac{\mathcal{E}_p E_R \sigma^2}{K} + BT_s \frac{\sigma^4}{2K^2}, \\ E[\dot{\zeta}^2(\tau_0)] &= \frac{2\sigma^4 B^2}{K^2}, \quad E[\zeta(\tau) \dot{\zeta}(\tau)] = 0 \end{aligned} \quad (8)$$

where  $E_R := \int_0^{T_s} p_R^2(t) dt$ . For  $K$  sufficiently large,  $\hat{\tau}_0$  in (4) will be close to the true timing offset  $\tau_0$ , and will lie in the interval  $[\tau_0 - \epsilon, \tau_0 + \epsilon]$  with probability close to 1, where  $\epsilon \ll T_p$  is a small positive number. Let us consider the two cases:  $\hat{\tau}_0 \in [\tau_0 - \epsilon, \tau_0]$  and  $\hat{\tau}_0 \in [\tau_0, \tau_0 + \epsilon]$ , separately. Starting with  $\hat{\tau}_0 \in [\tau_0, \tau_0 + \epsilon]$ , denoting  $\Delta\tau := \hat{\tau}_0 - \tau_0$ , and invoking Lagrange's mean value theorem, we know that there exists a  $\mu \in (0, 1)$  such that:  $\dot{J}_{\text{DA}}(\hat{\tau}_0) = \dot{J}_{\text{DA}}(\tau_0 + \Delta\tau) = \dot{J}_{\text{DA}}(\tau_0) + \Delta\tau \ddot{J}_{\text{DA}}(\tau_0 + \mu\Delta\tau)$ , where  $\dot{J}_{\text{DA}}(\tau)$  and  $\ddot{J}_{\text{DA}}(\tau)$  denote, respectively, the first and second derivatives of  $J_{\text{DA}}(\tau)$  with respect to  $\tau$ . Recalling that  $\dot{J}_{\text{DA}}(\hat{\tau}_0) = 0$  by the construction of  $\hat{\tau}_0$  in (4), we can write

$$\Delta\tau = -\frac{\dot{J}_{\text{DA}}(\tau_0)}{\ddot{J}_{\text{DA}}(\tau_0 + \mu\Delta\tau)}. \quad (9)$$

If  $\ddot{J}_{\text{DA}}(\tau_0 + \mu\Delta\tau)$  has nonzero mean  $\mathbf{E}[\ddot{J}_{\text{DA}}(\tau_0 + \mu\Delta\tau)]$ , which is asymptotically much greater than the perturbation:  $\ddot{J}_{\text{DA}}(\tau_0 + \mu\Delta\tau) - \mathbf{E}[\ddot{J}_{\text{DA}}(\tau_0 + \mu\Delta\tau)]$ , then  $\ddot{J}_{\text{DA}}(\tau_0 + \mu\Delta\tau)$  can be approximated by its mean; see, e.g., [7]. Applying this approximation to (9), the MSE of  $\hat{\tau}_0$  conditioned on the fact that  $\Delta\tau \in [0, \epsilon]$ , can be expressed as

$$\mathbf{E}[\Delta\tau^2 | \Delta\tau \in [0, \epsilon]] = \frac{\mathbf{E}[\dot{J}_{\text{DA}}^2(\tau_0)]}{\mathbf{E}^2[\ddot{J}_{\text{DA}}(\tau_0 + \mu\Delta\tau) | \Delta\tau \in [0, \epsilon]]}. \quad (10)$$

Using  $\bar{r}_s(t)$  from (6),  $\chi^2(\tau)$  for  $\tau \in [\tau_0, \tau_0 + \epsilon]$  in (7) can be manipulated further to arrive at

$$\begin{aligned} \chi^2(\tau) &= \mathcal{E}_p^2 \left\{ \int_0^{T_s} [p_R(t + \tau - \tau_0) + p_R(t - T_s + \tau - \tau_0)] \right. \\ &\quad \left. \times [-p_R(t + \tau - \tau_0) + p_R(t - T_s + \tau - \tau_0)] dt \right\}^2 \\ &= \mathcal{E}_p^2 \left[ \int_0^{\tau - \tau_0} p_R^2(t) dt - \int_{\tau - \tau_0}^{T_s} p_R^2(t) dt \right]^2. \end{aligned} \quad (11)$$

In the rest of this subsection, we evaluate (10) for data-aided TDT. Beginning with the denominator of (10), we differentiate (7) twice with respect to  $\tau$  to obtain

$$\begin{aligned} \ddot{J}_{\text{DA}}(\tau) &= 2\chi(\tau)\ddot{\chi}(\tau) + 2\dot{\chi}^2(\tau) \\ &\quad + 2\dot{\zeta}^2(\tau) + 2\zeta(\tau)\ddot{\zeta}(\tau) + \text{SNT} \end{aligned} \quad (12)$$

where SNT denotes single noise terms which vanish after taking expected values on both sides of (12). The expected values of the double noise terms in (12) decrease at least as  $\mathcal{O}(1/K)$  for large  $K$  (see (57) in Appendix II), which allows one to ignore them in the asymptotic regime. Based on (11) and (12), we can simplify  $\mathbb{E}[\ddot{J}_{\text{DA}}(\tau)]$  for  $\tau \in [\tau_0, \tau_0 + \epsilon]$  as follows:

$$\begin{aligned} \mathbb{E}[\ddot{J}_{\text{DA}}(\tau)] &= 2\chi(\tau)\ddot{\chi}(\tau) + 2\dot{\chi}^2(\tau) \\ &= 8\mathcal{E}_p^2 p_R(\tau - \tau_0)\dot{p}_R(\tau - \tau_0) \\ &\quad \times \left[ \int_0^{\tau - \tau_0} p_R^2(t) dt - \int_{\tau - \tau_0}^{T_s} p_R^2(t) dt \right] \\ &\quad + 8\mathcal{E}_p^2 p_R^4(\tau - \tau_0) \\ &= -8\mathcal{E}_p^2 E_R p_R(\tau - \tau_0)\dot{p}_R(\tau - \tau_0) \\ &\quad + 8\mathcal{E}_p^2 p_R^4(\tau - \tau_0), \quad \tau - \tau_0 \in [0, \epsilon] \end{aligned} \quad (13)$$

where the last step holds true because for  $\tau \in [\tau_0, \tau_0 + \epsilon]$ , we have

$$\int_0^{\tau - \tau_0} p_R^2(t) dt - \int_{\tau - \tau_0}^{T_s} p_R^2(t) dt \approx - \int_0^{T_s} p_R^2(t) dt = -E_R. \quad (14)$$

Substituting (13) into (9), we obtain

$$\Delta\tau = \frac{\dot{J}_{\text{DA}}(\tau_0)}{8\mathcal{E}_p^2 E_R p_R(\mu\Delta\tau)\dot{p}_R(\mu\Delta\tau) - 8\mathcal{E}_p^2 p_R^4(\mu\Delta\tau)}. \quad (15)$$

Close consideration of (15) will guide the choice of design parameters affecting the MSE of  $\hat{\tau}_0$ . Notice that if  $p(t)$  behaves like  $t^a$  for  $t \in [0, \epsilon]$ , then  $p(t)\dot{p}(t)$  behaves like  $at^{2a-1}$  and with  $a < 1/2$ , it follows that  $p(t)\dot{p}(t) \rightarrow \infty$  as  $t \rightarrow 0$ . Since the behavior of  $p_R(t)\dot{p}_R(t)$  near its end points (0 and  $T_s$ ) depends on how  $p(t)\dot{p}(t)$  behaves near its end points, we deduce that the appropriate  $p(t)$  can ensure  $p_R(t)\dot{p}_R(t) \rightarrow \infty$  as  $t \rightarrow 0$ , in which case  $\mathbb{E}[(\hat{\tau}_0 - \tau_0)^2] \rightarrow 0$ . So, a properly chosen pulse shaper can result in arbitrarily small asymptotic MSE of the TDT estimator. This observation motivates confining the class of desirable pulse shapers to satisfy the following property:

1) P1. *Monocycle pulse  $p(t)$  is continuous and differentiable over  $t \in (0, \epsilon]$ , and  $p(t) \propto t^a$  with  $a < 1/2$  for  $t \in [0, \epsilon]$ .*

Since  $p_R(t)\dot{p}_R(t)$  and  $p(t)\dot{p}(t)$  behave similarly near their end points, P1 implies that

$$p_R(\mu\Delta\tau)\dot{p}_R(\mu\Delta\tau) \propto a(\mu\Delta\tau)^{2a-1} \geq p_R(\epsilon)\dot{p}_R(\epsilon), \quad \text{for } \Delta\tau \in [0, \epsilon]. \quad (16)$$

The second term in the right-hand side of (13) is much smaller than the first term and can be neglected, since  $p_R(t) \approx 0$  near its end points. Using (16), the square of (15) is upper bounded

as

$$\mathbb{E}[(\hat{\tau}_0 - \tau_0)^2 | \Delta\tau \in [0, \epsilon]] \leq \frac{\mathbb{E}[\dot{J}_{\text{DA}}^2(\tau_0)]}{64\mathcal{E}_p^4 E_R^2 p_R^2(\epsilon)\dot{p}_R^2(\epsilon)}. \quad (17)$$

The numerator of (17) is found in Appendix III to be

$$\mathbb{E}[\dot{J}_{\text{DA}}^2(\tau_0)] = 4\chi^2(\tau_0)E[\dot{\zeta}^2(\tau_0)] = \frac{8}{K^2}\mathcal{E}_p^2 E_R^2 \sigma^4 B^2. \quad (18)$$

Substituting (18) into (17), we obtain

$$\mathbb{E}[(\hat{\tau}_0 - \tau_0)^2 | \Delta\tau \in [0, \epsilon]] \leq \frac{1}{K^2} \frac{(B\sigma^2)^2}{8\mathcal{E}_p^2 p_R^2(\epsilon)\dot{p}_R^2(\epsilon)}. \quad (19)$$

A similar approach can be followed when  $\Delta\tau \in [-\epsilon, 0]$ . Using the same arguments made for  $\tau \in [\tau_0, \tau_0 + \epsilon]$ , the counterpart of P1 is:

2) P2. *Monocycle pulse  $p(t)$  is continuous and differentiable over  $t \in (T_p - \epsilon, T_p]$ , and  $p(t) \propto (T_p - t)^b$  with  $b < 1/2$  for  $t \in [T_p - \epsilon, T_p]$ .*

Mimicking the steps used to derive (19), we find that for  $\tau \in [\tau_0 - \epsilon, \tau_0]$  it holds that

$$\mathbb{E}[(\hat{\tau}_0 - \tau_0)^2 | \Delta\tau \in [-\epsilon, 0]] \leq \frac{1}{K^2} \frac{(B\sigma^2)^2}{8\mathcal{E}_p^2 p_R^2(T_s - \epsilon)\dot{p}_R^2(T_s - \epsilon)}. \quad (20)$$

Combining (19) and (20), we arrive at

$$\begin{aligned} \mathbb{E}[\Delta\tau^2] &= \Pr(\Delta\tau \in [0, +\epsilon])\mathbb{E}[\Delta\tau^2 | \Delta\tau \in [0, +\epsilon]] \\ &\quad + \Pr(\Delta\tau \in [-\epsilon, 0])\mathbb{E}[\Delta\tau^2 | \Delta\tau \in [-\epsilon, 0]] \\ &\leq \Pr(\Delta\tau \in [0, +\epsilon]) \frac{\sigma^4 B^2}{K^2 8\mathcal{E}_p^2 p_R^2(\epsilon)\dot{p}_R^2(\epsilon)} \\ &\quad + \Pr(\Delta\tau \in [-\epsilon, 0]) \frac{\sigma^4 B^2}{K^2 8\mathcal{E}_p^2 p_R^2(T_s - \epsilon)\dot{p}_R^2(T_s - \epsilon)} \\ &\leq \frac{\sigma^4 B^2}{8\mathcal{E}_p^2 \min\{p_R^2(\epsilon)\dot{p}_R^2(\epsilon), p_R^2(T_s - \epsilon)\dot{p}_R^2(T_s - \epsilon)\}} \frac{1}{K^2} \end{aligned}$$

which we summarize as follows:

*Proposition 1:* For a pulse shaper  $p(t)$  designed to obey P1 and P2, the MSE of the DA-TDT estimator in (4) is asymptotically upper bounded by

$$\begin{aligned} \mathbb{E}[(\hat{\tau}_0 - \tau_0)^2] &\leq \frac{1}{K^2} \frac{B^2 \sigma^4}{8\mathcal{E}_p^2 \min\{p_R^2(\epsilon)\dot{p}_R^2(\epsilon), p_R^2(T_s - \epsilon)\dot{p}_R^2(T_s - \epsilon)\}}. \end{aligned} \quad (21)$$

Equation (21) reveals that  $\text{MSE}(\hat{\tau}_0) \rightarrow 0$  as  $K \rightarrow \infty$ , which proves mean-square sense consistency of the DA-TDT estimator. For large  $K$ , the estimator's convergence rate is at least on the order of  $\mathcal{O}(1/K^2)$ . Two remarks are now in order.

*Remark 1:* In deriving (21), we tacitly assumed that  $J_{\text{DA}}(\tau)$  has a unique maximum. Gaps present among successively received multipath components, cause  $J_{\text{DA}}(\tau)$  in (4) to exhibit a plateau around its peak. This implies multiple maxima and renders  $\hat{\tau}_0$  in (4) to have infinite mean square error. However, choosing *any* point on this plateau as our timing estimate leads

to maximum energy capture, which as far as symbol detection is concerned is what controls bit error rate (BER) in demodulation. From this point of view, albeit nonunique, any point on the plateau can be considered equally good, even though (21) will not be valid in this case.

*Remark 2:* To ensure the  $\mathcal{O}(1/K^2)$  convergence of  $\text{MSE}(\tau_0)$ , properties P1 and P2 are sufficient. However, for practical SNR values, conventional pulse shapers (not necessarily adhering to P1 and P2) also yield reliable timing estimators. This is confirmed by simulations, where second derivative of Gaussian pulse, which does not satisfy P1 and P2, is used as a UWB pulse shaper. Through simulations, it is illustrated that satisfactory MSE is obtained for practical values of  $K$  and SNR.

### B. Non-DA TDT

For the blind TDT estimator in (5), we can show that [ [23], (11)]

$$\mathbb{E}[J_{\text{NDA}}(\tau)] = \frac{1}{2}\chi^2(\tau) + \frac{1}{2}E_R^2 + E[\zeta^2(\tau)]. \quad (22)$$

To evaluate (10) for  $J_{\text{NDA}}(\tau)$ , we follow steps similar to those used for DA-TDT. Specifically,  $\mathbb{E}[\ddot{J}_{\text{NDA}}(\tau)]$  for  $\tau \in [\tau_0, \tau_0 + \epsilon]$  can be expressed as

$$\begin{aligned} \mathbb{E}[\ddot{J}_{\text{NDA}}(\tau)] &= 2\chi(\tau)\ddot{\chi}(\tau) + 2\dot{\chi}^2(\tau) \\ &= 4\mathcal{E}_p^2 p_R(\tau - \tau_0)\dot{p}_R(\tau - \tau_0) \\ &\quad \times \left[ \int_0^{\tau - \tau_0} p_R^2(t) dt - \int_{\tau - \tau_0}^{T_s} p_R^2(t) dt \right] \\ &\quad + 4\mathcal{E}_p^2 p_R^4(\tau - \tau_0) \\ &= -4\mathcal{E}_p^2 E_R p_R(\tau - \tau_0)\dot{p}_R(\tau - \tau_0) \\ &\quad + 4\mathcal{E}_p^2 p_R^4(\tau - \tau_0). \end{aligned} \quad (23)$$

Using an approach similar to Appendix III, we find

$$\mathbb{E}\left[\dot{J}_{\text{NDA}}^2(\tau_0)\right] = \frac{4}{K}\chi^2(\tau_0)E\left[\dot{\zeta}_a^2(\tau_0)\right] = \frac{8}{K}\mathcal{E}_p^2 E_R^2 \sigma^4 B^2 \quad (24)$$

where  $\zeta_a$  is defined similar to  $\zeta$ , but with all terms containing  $\bar{\eta}$  in (7) replaced by  $\eta$ . Variance expressions for  $\zeta_a$  can also be derived from those of  $\zeta$  in (8) after replacing  $\sigma^2/K$  with  $\sigma^2$ . Substituting (23) and (24) in (10) and applying P1 and P2, a result similar to DA-TDT is obtained which we summarize next.

*Proposition 2:* For a pulse shaper  $p(t)$  designed to satisfy P1 and P2, the MSE of the non-DA TDT estimator in (5) is asymptotically upper bounded by

$$\begin{aligned} &\mathbb{E}[(\hat{\tau}_0 - \tau_0)^2] \\ &\leq \frac{1}{K} \frac{B^2 \sigma^4}{2\mathcal{E}_p^2 \min\{p_R^2(\epsilon)\dot{p}_R^2(\epsilon), p_R^2(T_s - \epsilon)\dot{p}_R^2(T_s - \epsilon)\}}. \end{aligned} \quad (25)$$

Notice that again  $\text{MSE} \rightarrow 0$  as  $K \rightarrow \infty$ , which proves consistency of our blind TDT estimator. For large  $K$ , its convergence rate will be at least on the order of  $\mathcal{O}(1/K)$ , which is

an order of magnitude slower than its counterpart for DA-TDT. Having quantified the asymptotic TDT acquisition performance, we move on to see how the  $\hat{\tau}$  estimators can be used for demodulation.

## IV. TDT-BASED DEMODULATION

In this section, we will derive a TDT-based demodulator and study its performance. Our exposition will proceed in four parts: Template recovery from  $r(t)$ ; TDT-based demodulation performance in the presence of timing errors (large sample analysis); Finite sample analysis of TDT-based demodulation in the presence of timing errors; and Comparisons between RAKE and TDT-based receivers with perfect timing.

### A. Template Recovery

1) *DA Operation:* Obtained using the training sequence  $\{s(n) = (-1)^{\lfloor n/2 \rfloor}\}$ , the waveform  $\tilde{r}(t)$  in (3) conveys information (within a circular shift  $\tau_0$ ) about the received aggregate template  $p_R(t)$ . With  $\hat{\tau}_0$  obtained as in (4), simple timing adjustment of  $\tilde{r}(t)$  yields

$$\check{p}_{R,\text{DA}}(t) = \frac{1}{\sqrt{\mathcal{E}_p}} \tilde{r}(t + \hat{\tau}_0), \quad t \in [0, T_s]. \quad (26)$$

Since  $\tilde{r}(t)$  is required for TDT acquisition, the complexity in forming  $\check{p}_{R,\text{DA}}(t)$  is minimal. But as we explain in Appendix I,  $\check{p}_{R,\text{DA}}(t)$  recovered through  $\tilde{r}(t)$  has a sign ambiguity. To resolve this ambiguity, a couple of additional positive training symbols  $\{s(k) = +1\}_{k=K_1}^{K_2}$  can be transmitted and demodulated using

$$\hat{s}(k) = \text{sign} \left[ \int_{kT_s + \hat{\tau}_0}^{(k+1)T_s + \hat{\tau}_0} r(t)\check{p}_{R,\text{DA}}(t - kT_s - \hat{\tau}_0) dt \right] \quad (27)$$

for  $k \in [K_1, K_2]$ . Through averaging, we can find a more reliable sign estimator via  $\text{sign}[\sum_{k=K_1}^{K_2} \hat{s}(k)]$ . And based on the latter, we can obtain the ambiguity-free aggregate received template as:

$$\hat{p}_{R,\text{DA}}(t) = \check{p}_{R,\text{DA}}(t) \cdot \text{sign} \left[ \sum_{k=K_1}^{K_2} \hat{s}(k) \right], \quad t \in [0, T_s]. \quad (28)$$

Since  $K$  used for TDT-based acquisition is relatively large, the additional training symbols contribute a negligible amount to the overall overhead and can be neglected.

2) *Blind Operation:* Consider a broadcast scenario where node A transmits data to node C. Suppose node B wants to establish a new link with A. To synchronize B, A has to interrupt transmission to C and send a training pattern. A training pattern must be repeated for every node who joins the broadcast, and transmitting it wastes power and data rate. A more efficient approach is for B to synchronize with A and recover a demodulation template without interrupting the A–C communication. For such a scenario, we develop a blind template recovery algorithm to operate jointly with blind TDT. To recover a demodulation template without training, we will use  $s(n)$  drawn

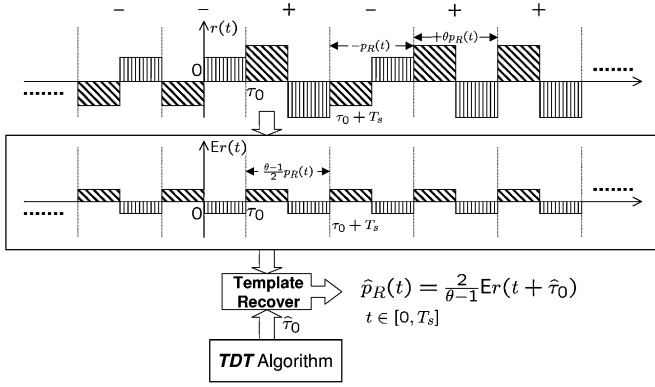


Fig. 1. Template recovery in non-DA TDT with asymmetric-PAM.

from a binary asymmetric PAM (A-PAM), where information bearing symbols are  $s(n) = 2b(n) - 1 + 2\theta\delta(b(n) - 1)$ , with bits  $b(n)$  taking values  $\{0, 1\}$  equiprobably;  $\theta > 0$  is the A-PAM parameter; and,  $\delta(\cdot)$  denotes Kronecker's delta function. As in [13], taking expectation of the received signal in (2) produces  $\mathbb{E}[r(t)] = \sqrt{\mathcal{E}_p}\theta \sum_k p_R(t - kT_s - \tau_0)$ ; see also Fig. 1. If  $\tau_0$  were available, the received symbol waveform could be easily obtained as:  $p_R(t) = \mathbb{E}[r(t + \tau_0)]/(\sqrt{\mathcal{E}_p}\theta)$ . In practice, the ensemble mean is replaced by its consistent sample mean estimator, and  $\tau_0$  is replaced by  $\hat{\tau}_0$  to obtain the synchronized aggregate template (SAT) as

$$\hat{p}_{R,\text{NDA}}(t) = \frac{1}{\sqrt{\mathcal{E}_p}\theta} \frac{1}{2K} \sum_{k=0}^{2K-1} r(t + kT_s + \hat{\tau}_0) \quad t \in [0, T_s] \quad (29)$$

where an averaging size of  $2K$  is used, since  $2K$  symbols are needed in (5) for TDT-based acquisition. Without sacrificing spectral efficiency, (29) yields an estimate of the demodulation template without sign ambiguity. Although (29) is similar to the one proposed in [12], [13] for joint timing synchronization and demodulation, one difference is that [12], [13] advocates A-PAM transmission intermittently to enable timing acquisition, whereas here we rely on A-PAM only for SAT recovery and acquire timing using the non-DA TDT estimator in (5).

### B. Large Sample Performance

Large sample performance of TDT-based demodulators in the presence of timing errors is considered here, while a finite sample performance analysis is carried out in Section IV-C. Let us define  $\tilde{\tau}_0 := \hat{\tau}_0 - \tau_0$ . Throughout this section and the next, we assume without loss of generality that  $|\tilde{\tau}_0| \in [0, T_s]$ . If  $|\tilde{\tau}_0| \geq T_s$ , a delay of several  $T_s$  secs in symbol detection will be in effect. Nonetheless, the figures of merit for our analysis (BER and detection SNR) will remain the same.

With  $\tilde{\tau}_0 \in [0, T_s]$ , as the number of samples  $K$  in (3) and (29) grows large, the SAT recovered either from (26) or from (29) will asymptotically converge to the template

$$\hat{p}_R(t) = p_R(t + \tilde{\tau}_0) + p_R(t - T_s + \tilde{\tau}_0), \quad t \in [0, T_s]. \quad (30)$$

Utilizing  $\hat{p}_R(t)$ , we obtain the decision variable

$$\begin{aligned} d_k &= \int_0^{T_s} \hat{p}_R(t) r(t + kT_s + \hat{\tau}_0) dt \\ &= \sqrt{\mathcal{E}_p} s(k) E_C(\tilde{\tau}_0) + \sqrt{\mathcal{E}_p} s(k+1) E_C(\tilde{\tau}_0 - T_s) + \eta_k \end{aligned} \quad (31)$$

where  $E_C(u) := \int_0^{T_s} p_R^2(t+u) dt$  denotes the amount of captured energy, and  $\eta_k := \int_0^{T_s} \eta(t + kT_s + \hat{\tau}_0) \hat{p}_R(t) dt$ . It is easily seen that  $\eta_k$  is zero mean Gaussian with variance  $\sigma^2 \int_0^{T_s} \hat{p}_R^2(t) dt/2 = \sigma^2 E_R/2$ , where  $E_R$  denotes the total received energy defined in (14). Thus, the probability of error for the sign detector  $\hat{s}(k) = \text{sign}[d_k]$  as  $K \rightarrow \infty$  can be evaluated as

$$\begin{aligned} P_e^\infty &= \frac{1}{4} \Pr(d_k < 0 | s(k) = +1, s(k+1) = +1) \\ &\quad + \frac{1}{4} \Pr(d_k < 0 | s(k) = +1, s(k+1) = -1) \\ &\quad + \frac{1}{4} \Pr(d_k > 0 | s(k) = -1, s(k+1) = +1) \\ &\quad + \frac{1}{4} \Pr(d_k > 0 | s(k) = -1, s(k+1) = -1) \\ &= \frac{1}{2} \left[ Q \left( \sqrt{\frac{2\mathcal{E}_p E_R}{\sigma^2}} \right) \right. \\ &\quad \left. + Q \left( \sqrt{\frac{2\mathcal{E}_p E_R}{\sigma^2}} \frac{E_C(\tilde{\tau}_0) - E_C(\tilde{\tau}_0 - T_s)}{E_R} \right) \right]. \end{aligned} \quad (32)$$

Similarly, when  $\tilde{\tau}_0 \in [-T_s, 0]$ , the BER of the sign detector can be found to be

$$\begin{aligned} P_e^\infty &= \frac{1}{2} \left[ Q \left( \sqrt{\frac{2\mathcal{E}_p E_R}{\sigma^2}} \right) \right. \\ &\quad \left. + Q \left( \sqrt{\frac{2\mathcal{E}_p E_R}{\sigma^2}} \frac{E_C(\tilde{\tau}_0) - E_C(\tilde{\tau}_0 + T_s)}{E_R} \right) \right]. \end{aligned} \quad (33)$$

From (32) and (33), one can clearly see that our demodulator will be very robust to mistiming  $\tilde{\tau}_0$ , so long as  $E_C(\tilde{\tau}_0)$  captures most of  $E_R$ .

### C. Finite Sample Performance

Because BER in the presence of mistiming is difficult to evaluate with finite samples, we will derive an expression for the predetection SNR. Assuming data-aided operation and correct removal of sign ambiguity in (28), the decision variable is formed as follows:

$$(d_k)_{\text{TDT}} = \int_0^{T_s} \hat{p}_{R,\text{DA}}(t) r(t + kT_s + \hat{\tau}_0) dt. \quad (34)$$

Supposing temporarily that  $\tilde{\tau}_0 = \hat{\tau}_0 - \tau_0 \in [0, T_s]$ , for  $t \in [0, T_s]$ , the SAT and received waveform can be respectively

expressed as [cf. (2), (6), and (26)]

$$\begin{aligned}\hat{p}_{R,DA}(t) &= \sum_{l=-1}^0 p_R(t + \tilde{\tau}_0 + lT_s) + \frac{1}{\sqrt{\mathcal{E}_p}} \bar{\eta}(t + \hat{\tau}_0) \\ r(t + kT_s + \hat{\tau}_0) &= \sqrt{\mathcal{E}_p} \sum_{l=-1}^0 s(k-l) p_R(t + \tilde{\tau}_0 + lT_s) \\ &\quad + \eta(t + kT_s + \hat{\tau}_0).\end{aligned}\quad (35)$$

Substituting (35) into (34), we obtain

$$\begin{aligned}(d_k)_{\text{TDT}} &= \sqrt{\mathcal{E}_p} s(k) \int_0^{T_s} p_R^2(t + \tilde{\tau}_0) dt \\ &\quad + \sqrt{\mathcal{E}_p} s(k+1) \int_0^{T_s} p_R^2(t - T_s + \tilde{\tau}_0) dt \\ &\quad + \int_0^{T_s} p_R(t + \tilde{\tau}_0) \\ &\quad \times [\eta(t + kT_s + \hat{\tau}_0) + s(k)\bar{\eta}(t + \hat{\tau}_0)] dt \\ &\quad + \int_0^{T_s} p_R(t - T_s + \tilde{\tau}_0) \\ &\quad \times [\eta(t + kT_s + \hat{\tau}_0) + s(k+1)\bar{\eta}(t + \hat{\tau}_0)] dt \\ &\quad + \int_0^{T_s} \frac{1}{\sqrt{\mathcal{E}_p}} \eta(t + kT_s + \hat{\tau}_0) \bar{\eta}(t + \hat{\tau}_0) dt \\ &:= \sqrt{\mathcal{E}_p} [s(k)E_C(\tilde{\tau}_0) + s(k+1)E_C(\tilde{\tau}_0 - T_s)] \\ &\quad + \bar{\eta}_1(k) + \bar{\eta}_2(k) + \bar{\eta}_3(k)\end{aligned}\quad (36)$$

where  $\bar{\eta}_1(k)$ ,  $\bar{\eta}_2(k)$ , and  $\bar{\eta}_3(k)$  are mutually uncorrelated zero-mean Gaussian with variances  $\text{Var}(\bar{\eta}_1) = [E_C(\tilde{\tau}_0)\sigma^2(K+1)]/(2K)$ ,  $\text{Var}(\bar{\eta}_2) = [E_C(\tilde{\tau}_0 - T_s)\sigma^2(K+1)]/(2K)$ , and  $\text{Var}(\bar{\eta}_3) = (BT_s\sigma^4)/(2K\mathcal{E}_p)$ . Let  $N_1 := \text{Var}(\bar{\eta}_1(k)) + \text{Var}(\bar{\eta}_2(k)) + \text{Var}(\bar{\eta}_3(k))$ . The signal-to-interference-plus-noise-ratio (SINR) in (36) is then found as

$$\begin{aligned}\text{SINR}_{\text{TDT}} &= \frac{\mathbb{E}[(\sqrt{\mathcal{E}_p}E_C(\tilde{\tau}_0)s(k))^2]}{\mathbb{E}[(\sqrt{\mathcal{E}_p}E_C(\tilde{\tau}_0 - T_s)s(k+1))^2] + N_1} \\ &= \frac{E_C^2(\tilde{\tau}_0)}{E_C^2(\tilde{\tau}_0 - T_s) + \left(\frac{\sigma^2}{\mathcal{E}_p}\right)\left(\frac{(K+1)E_R}{2K}\right) + \left(\frac{\sigma^2}{\mathcal{E}_p}\right)^2\left(\frac{BT_s}{2K}\right)}.\end{aligned}\quad (37)$$

Similarly, when  $\tilde{\tau}_0 \in [-T_s, 0]$ , the SINR turns out to be

$$\begin{aligned}\text{SINR}_{\text{TDT}} &= \frac{E_C^2(\tilde{\tau}_0)}{E_C^2(\tilde{\tau}_0 + T_s) + \left(\frac{\sigma^2}{\mathcal{E}_p}\right)\left(\frac{(K+1)E_R}{2K}\right) + \left(\frac{\sigma^2}{\mathcal{E}_p}\right)^2\left(\frac{BT_s}{2K}\right)}.\end{aligned}\quad (38)$$

As with our large sample analysis, (37) and (38) imply that our demodulator will be very robust to mistiming  $\tilde{\tau}_0$ , as long as  $E_C(\tilde{\tau}_0)$  captures most of  $E_R$ .

#### D. RAKE Versus TDT-Based Demodulation

With frequency-selective propagation, RAKE offers a low-complexity demodulator capable of collecting the channel's multipath energy. However, RAKE performance in the UWB regime is limited mainly because only a small fraction of multipath energy can be captured with a small number of fingers that can be afforded by implementation constraints. TDT-based demodulation on the other hand, can capture the full multipath energy while bypassing the costly estimation of UWB channels which is required for RAKE operation. A comparison of these two schemes is thus well motivated, and will shed light into TDT versus RAKE capabilities and shortcomings. For a fair comparison, the timing offset is assumed to be perfectly known for both demodulators; i.e., throughout this section we consider  $\hat{\tau}_0 = \tau_0$ .

1) *RAKE Performance*: To enable coherent detection, a RAKE receiver requires estimation of the  $L+1$  tap weights and delays of the channel, which is typically performed using a training sequence. The  $L_r \ll L+1$  strongest weights are then selected to form the RAKE demodulation template. To simplify exposition, let us suppose that: i) tap delays are perfectly estimated; ii)  $T_p$  is chosen small enough to avoid inter pulse interference; and, iii) the TDT-TH code is absent. ML estimation of the tap weights relies on  $N_{\text{RAKE}}$  positive training symbols for which the aggregate transmitted waveform can be written as  $s_{\text{TR}}(t) = \sqrt{\mathcal{E}_p} \sum_{i=1}^{N_{\text{RAKE}}} p_T(t - iT_s)$ . The resultant DA tap estimators are given by [11]

$$\begin{aligned}\hat{\alpha}_l &= \frac{1}{N_{\text{RAKE}}N_f\sqrt{\mathcal{E}_p}} \\ &\quad \times \int r(t) \left( \sum_{i=1}^{N_{\text{RAKE}}} p_T(t - iT_s - \tau_{l,0}) \right) dt\end{aligned}\quad (39)$$

for  $l \in \mathcal{S}(L_r)$ , where  $\mathcal{S}(L_r)$  is the set of  $L_r$  strongest multipath components, each with variance

$$\text{Var}(\hat{\alpha}_l) = \frac{\sigma^2}{2N_{\text{RAKE}}N_f\mathcal{E}_p}.\quad (40)$$

A RAKE receiver with maximal ratio combining (MRC) just forms the demodulation template  $\hat{h}(t) = \sum_{l \in \mathcal{S}(L_r)} \hat{\alpha}_l p_T(t - \tau_{l,0})$ , and obtains the decision statistic as

$$(d_k)_{\text{RAKE}} = \int_0^{T_s} r(t + kT_s + \tau_0) \hat{h}(t) dt.\quad (41)$$

Let  $\hat{\alpha}_l = \alpha_l + n_l$ , where  $n_l$  is zero-mean Gaussian with variance defined in (40). Substituting (2) and  $\hat{h}(t) = \sum_{l \in \mathcal{S}(L_r)} \hat{\alpha}_l p_T(t - \tau_{l,0})$  into (41), we obtain

$$\begin{aligned}(d_k)_{\text{RAKE}} &= s(k)N_f\sqrt{\mathcal{E}_p} \sum_{l \in \mathcal{S}(L_r)} \alpha_l^2 \\ &\quad + s(k)N_f\sqrt{\mathcal{E}_p} \sum_{l \in \mathcal{S}(L_r)} \alpha_l n_l \\ &\quad + \int_0^{T_s} \eta(t + kT_s + \tau_0) \hat{h}(t) dt.\end{aligned}\quad (42)$$

Since  $n_l$  and  $\eta(t)$  are independent, the variance of the noise terms in the RHS of (42) can be evaluated easily, based on which the SNR at the RAKE output can be expressed as

$$\text{SNR}_{\text{RAKE}} = \left\{ \frac{N_{\text{RAKE}} N_f \left( \sum_{l \in \mathcal{S}(L_r)} \alpha_l^2 \right) + 1}{2 N_{\text{RAKE}} N_f^2 \left( \sum_{l \in \mathcal{S}(L_r)} \alpha_l^2 \right)^2} (\sigma^2 / \mathcal{E}_p) + \frac{L_r}{4 N_f^2 N_{\text{RAKE}} \left( \sum_{l \in \mathcal{S}(L_r)} \alpha_l^2 \right)^2} (\sigma^2 / \mathcal{E}_p)^2 \right\}^{-1}. \quad (43)$$

We are now ready to compare RAKE with DA-TDT based demodulation in terms of detection SNR when finite sample detection is used, and perfect timing is assumed for both receivers. For DA-TDT, plugging  $\tilde{\tau}_0 = 0$  in (37) or (38) gives

$$\text{SNR}_{\text{TDT}} = \frac{2 \mathcal{E}_p N_f \sum_{i=0}^L \alpha_i^2}{\sigma^2} \times \left( 1 + \frac{B T_s}{K} \frac{\sigma^2}{\mathcal{E}_p N_f \sum_{i=0}^L \alpha_i^2} \right)^{-1}. \quad (44)$$

Upon defining  $(\sum_{l \in \mathcal{S}(L_r)} \alpha_l^2) / (\sum_{i=0}^L \alpha_i^2) := \beta$ , we correspondingly have from (43) that

$$\text{SNR}_{\text{RAKE}} = \frac{2 \mathcal{E}_p N_f \sum_{i=0}^L \alpha_i^2}{\sigma^2} \times \left( 1 + \frac{L_r}{2 N_{\text{RAKE}} \mathcal{E}_p N_f \beta \sum_{i=0}^L \alpha_i^2} \right)^{-1} \beta. \quad (45)$$

Comparing (44) with (45), we deduce the following:

- 1) Because of the noise enhancement arising due to the large time-bandwidth product  $B T_s$  in (44), for small  $K$ , RAKE may outperform DA-TDT. But remember that here we assumed the RAKE finger delays (which are not needed by TDT) are available error-free.
- 2) When  $K$  is large enough, TDT will outperform the RAKE, since TDT-based demodulation collects all the available multipath energy while RAKE with a small number of fingers  $L_r \ll L$  has limited capability in capturing the ample energy produced by the dense multipath of the UWB channel.

*Remark 3:* Transmitted reference (TR) is an alternative UWB demodulator, which has been also compared with RAKE recently [3]. In its DA mode, our TDT-based scheme basically performs TR demodulation. However, there are two major benefits that a TDT-based receiver offers over TR: i) Similar to RAKE, TR requires a timing offset estimate to be available beforehand, while the symbol-long templates in the TDT-based receiver are utilized both for timing and demodulation; and ii) TR suffers from a 50% rate loss [5], while TDT incurs no overhead in its blind mode, and a very small rate loss in the DA mode as it requires  $2K$  training symbols only at the beginning

of every block. For typical values of the channel coherence time, the number of these training symbols are less than 1% of the block size [12]. As for the blind TDT mode, the price paid is a somewhat longer acquisition interval.

As an alternative to blind TDT, the ensuing session will introduce a tracking loop operating in a decision-directed (DD) mode in order to follow channel and timing offset variations.

## V. TLL DESIGN AND ANALYSIS

After timing has been successfully acquired, a tracking subsystem is required to track changes in timing offset  $\tau_0(t)$  arising from relative motion between transmitter and receiver and/or clock drifts present in transmit-receive oscillators. In this section, we will develop a time lock loop (TLL) to follow these time variations. With  $B_L$  denoting the noise equivalent bandwidth of the TLL, we will further select the loop parameters to minimize the weighted sum of the output noise power and its transient error energy for a predetermined TLL input signal. We will assume the following operating conditions:

- 1) c1. Acquisition has proceeded TLL operation and it has been successful so that the TLL is “in lock” at the beginning of its operation.
- 2) c2. Monocycle pulse  $p(t)$  is known at the receiver.
- 3) c3. For Gaussian pulse and its derivatives of duration  $T_p \approx 0.3$  nsec or smaller, [2] has shown that the effect of multipath, with multipath parameters defined in [8], on the tracking loop is negligible and can be ignored. Thus for tracking loop analysis, UWB multipath channel can be modeled as only producing a single scaled and delayed replica of the transmitted signal.
- 4) c4. UWB channel parameters change slowly with time.

Since TLL is already in lock under c1, it suffices to track only the first arriving multipath component of each symbol. Condition c3 ensures that ignoring other multipath components does not degrade loop performance. TLL operates in a DD fashion and makes use of the detected symbols which are reliable when TLL is in lock. To design the TLL, we will pursue an ML approach. With  $\hat{\tau}_k$  denoting the TLL estimate of  $\tau_0(k)$  at time  $kT_s$ , the error signal  $e(k)$  which drives the loop is given by (see e.g., [14])

$$\begin{aligned} e(k) &= -\hat{s}(k) \int r(t) \dot{p}(t - kT_s - \hat{\tau}_k) dt \\ &= \hat{s}(k) (r(t) \star [-\dot{p}(-t)])|_{t=kT_s + \hat{\tau}_k} \end{aligned} \quad (46)$$

where  $\star$  denotes convolution, and  $\{\hat{s}(k)\}$  denotes previously detected symbols. A hybrid TLL is used, as depicted in Fig. 2, where the loop operates digitally and sampling is performed synchronously by the number controlled oscillator (NCO) at the symbol rate  $T_s$  [4]. The factor  $1/\hat{\alpha}_1$  in Fig. 2 is required in order to eliminate the effect of  $\alpha_1$  which is a time varying random quantity accounting for channel effect on the first arriving pulse, and has an undesirable impact on the loop operation [2]. The estimator  $\hat{\alpha}_1$  can be obtained using a DD version

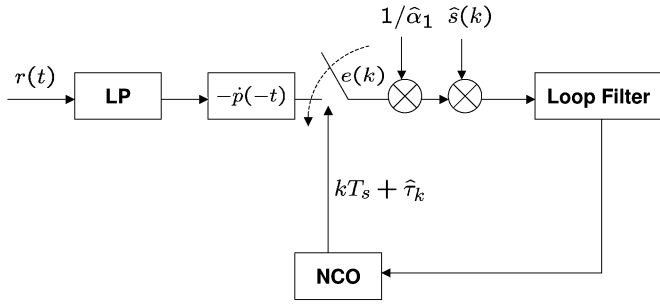


Fig. 2. Block diagram of TLL.

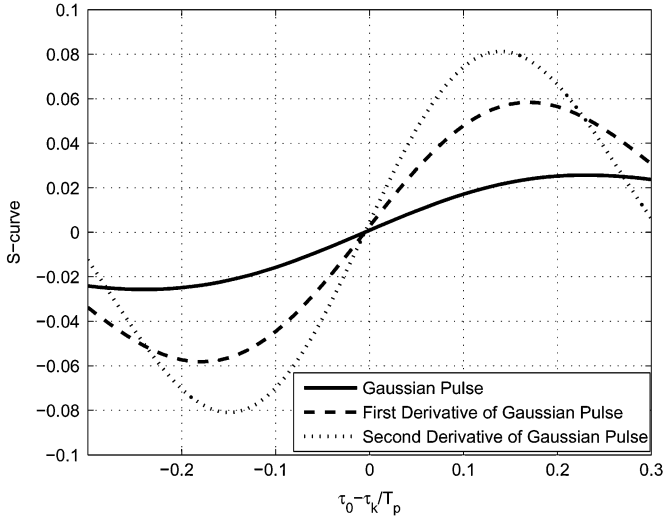


Fig. 3. S-curve for the Gaussian monocycle and its first and second derivatives.

of (39)

$$\hat{\alpha}_1(k) = \frac{1}{MN_f \sqrt{\mathcal{E}_p}} \int r(t) \times \left( \sum_{i=k-M}^{k-1} \hat{s}(i) p_T(t - iT_s - \hat{\tau}_{k-1}) \right) dt$$

where  $k$  is the index denoting time  $t = kT_s$ ,  $M$  is the averaging size, and  $\hat{\tau}_{k-1}$  is the loop estimate of  $\tau_0(k-1)$  at  $t = (k-1)T_s$ . The so called S-curve,  $\mathbf{E}[e(k)]$ , is found from (46) to be

$$g(\Delta\tau_k) := \mathbf{E}[e(k)] = \sqrt{\mathcal{E}_p} p(t) \star [-\dot{p}(-t)]|_{t=-(\tau_0(k) - \hat{\tau}_k)} := \sqrt{\mathcal{E}_p} R_{p\dot{p}}(-\Delta\tau_k) \quad (47)$$

where  $\Delta\tau_k := \tau_0(k) - \hat{\tau}_k$  and  $R_{p\dot{p}}(t) := p(t) \star [-\dot{p}(-t)]$ . The S-curve for a Gaussian monocycle pulse  $p(t)$  and its first and second derivatives are plotted in Fig. 3. The second derivative of the Gaussian monocycle has the highest slope near the origin, and is thus most sensitive to small timing errors. On the other hand, the Gaussian pulse offers the largest lock range. To analyze the loop tracking performance, the TLL is assumed operating close to  $\Delta\tau_k = 0$ , in which case  $g(\Delta\tau_k)$  can be linearized as  $g(\Delta\tau_k) = g(0) + \dot{g}(0)\Delta\tau_k$ . Fig. 4 depicts the equivalent linear model in which  $G := \dot{g}(0) = \sqrt{\mathcal{E}_p} R_{p\dot{p}}(0)$ , and  $\eta_k := e(k) -$

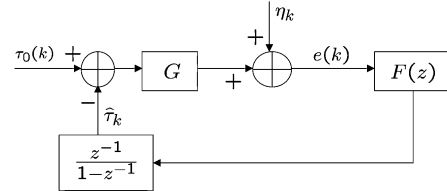


Fig. 4. Linearized TLL model.

$\mathbf{E}[e(k)]$  is the noise entering the loop. It follows easily from (46) and (2) that

$$\eta_k = -\frac{\hat{s}(k)}{\hat{\alpha}_1(k)} \int \eta(t) \dot{p}(t - kT_s - \hat{\tau}_k) dt. \quad (48)$$

Noise sequence  $\eta_k$  is white with variance  $\sigma^2 \mathcal{E}_p / 2\mathbf{E}[\hat{\alpha}_1^2(k)]$ , where  $\mathcal{E}_p := \int [\dot{p}(t)]^2 dt$ , and  $\mathbf{E}[\hat{\alpha}_1^2(k)]$  is considered much greater than the perturbation  $\hat{\alpha}_1^2(k) - \mathbf{E}[\hat{\alpha}_1^2(k)]$ . The loop filter is selected to track a ramp input with zero steady-state error [15]. From Fig. 4, the loop transfer function can be written as

$$H_{\text{loop}}(z) = \frac{T(z)}{N(z)} = \frac{K_D z + K_D \kappa}{z^2 + (GK_D - 2)z + (GK_D \kappa + 1)} \quad (49)$$

where  $T(z)$  and  $N(z)$  are the z-transforms of  $\tau_k$  and  $\eta_k$ , respectively, and  $F(z) := K_D(z + \kappa)/(z - 1)$ . Constants  $K_D$  and  $\kappa$  are design parameters which we will choose later on to optimize loop performance. Using standard z-transform techniques, the noise power at the output of the TLL ( $\hat{\tau}_k$  in Fig. 4) is found to be [cf. (48), (49), and [10, Table IV)]

$$\sigma_\tau^2 = \frac{\sigma^2 \mathcal{E}_p}{2\mathbf{E}[\hat{\alpha}_1^2(k)]} \times \left| \frac{(1 + \kappa^2)(2 + GK_D \kappa) - 2\kappa(GK_D - 2)}{G\kappa[G^2 K_D(\kappa^2 - 1) + 4G(\kappa + 1)]} \right|. \quad (50)$$

Choosing  $K_D$  and  $\kappa$  to minimize (50) trades off noise performance for transient response of the loop. To determine  $K_D$  and  $\kappa$ , we will use a result from analog PLLs to jointly optimize loop performance with respect to transient behavior as well as noise handling ability. To this end, we need to map  $z$ -domain quantities to the  $s$ -domain. Letting  $H_{\text{loop}}(z)$  model a lowpass filter with noise equivalent bandwidth  $B_L \ll 1/T_s$ , a digital PLL approximates an analog PLL with  $z = e^{j\omega T_s} \approx 1 + j\omega T_s$ , for  $\omega T_s \ll 1$ . Setting  $j\omega = s$ , we can write  $H_{\text{loop}}(z)$  as

$$H_{\text{loop}}(s) = \frac{1}{G} \times \frac{s \left( \frac{T_s}{1+\kappa} \right) + 1}{s^2 \left( \frac{T_s^2}{GK_D(1+\kappa)} \right) + s \left( \frac{T_s}{1+\kappa} \right) + 1} \quad (51)$$

where  $z = 1 + sT_s$ . For a given TLL input  $\tau_0(t)$ , the optimization method we use minimizes the noise MSE at the TLL output subject to a finite transient error energy constraint [9]: The Lagrangian is formed as  $\sigma_\tau^2 + \lambda^2 \int_0^\infty [\tau_0(t) - \tau(t)]^2 dt$ , where the Lagrange multiplier  $\lambda$  can be thought of as a relative weight between noise MSE and transient error energy. For a ramp input  $\tau_0(t) = mt$ , the optimal loop parameters can be found as (see

(51) and [15, Table 3.7-1])

$$\omega_n^2 = m\lambda(\text{Var}(\eta_k))^{-1/2}, \kappa = \frac{\omega_n T_s}{\sqrt{2}} - 1, \quad K_D = \frac{\sqrt{2}\omega_n T_s}{G}. \quad (52)$$

The remaining task is to check for condition  $B_L \ll 1/T_s$ , which was used in deriving (51) from (49). Parameter  $B_L$  is defined as [15]

$$B_L = \frac{1}{H_{\text{loop}}^2(0)} \int_0^\infty |H_{\text{loop}}(f)|^2 df.$$

For  $H_{\text{loop}}(s)$  in (51),  $B_L$  is found to be  $B_L = 0.53\omega_n \ll 1/T_s$  [15, Table 3.3-1].

The TLL design procedure can now be summarized as follows:

**TLL Design.** For an input ramp  $\tau_0(t) = mt$ , find  $\omega_n$  as in (52) and check whether  $B_L = 0.53\omega_n \ll 1/T_s$  holds true. If it holds, compute  $K_D$  and  $\kappa$  from (52), and build the TLL as in Fig. 2.

If the step or ramp error is large enough, it can drive the TLL out of lock. TLL lock range depends on the monocycle shape  $p(t)$ , but can not exceed  $2T_p$ . UWB transceivers use monocycles of ultra short duration so the lock range is usually small (in the order of ns), meaning that TLL can easily fall out of lock. In UWB channels, the received waveform consists of a large number of resolvable paths, so when out of lock, TLL begins to track a wrong path instead of the first one. Fortunately, the fact that TDT-based demodulators are robust to mistiming implies that if TLL is following a path close to the first one, the TDT-based demodulator can still perform reliable symbol detection. A lock detector which measures predetection power and compares it versus a threshold can be used to prevent false locks far away from the correct path by producing an “out of lock” signal. After the generation of such a signal, the receiver enters the acquisition mode. Using DA or blind TDT acquisition, the TLL is brought back in lock, and resumes its operation.

Because of c4, the template used in TDT-based demodulation should be updated continuously to account for channel variations. This can be done by averaging the received analog waveform  $r(t)$  in a manner similar to (3), but in a DD mode. If  $\{\hat{s}(k)\}$  denotes the detected symbols,  $K$  the averaging size, and  $\hat{\tau}_n$  stands for the TLL estimate of  $\tau_0$  at time  $nT_s$ , then the demodulation template denoted by  $\hat{p}_{n,R}(t)$  is evaluated at time  $nT_s$  by a moving average

$$\hat{p}_{n,R}(t) = \frac{1}{K} \sum_{k=n-K+1}^n \hat{s}(k)r(t + kT_s + \hat{\tau}_n), \quad t \in [0, T_s].$$

UWB radios are mainly considered for indoor wireless communications, where speeds are not that high (on the order of 1 m/s). As a result, channel coherence times are on the order of 21 msec [12]; so, updating our timing and demodulation template estimates every symbol period, which is usually less than 1  $\mu\text{sec}$ , is good enough.

In a block diagram format, Fig. 5 summarizes the acquisition, demodulation and tracking modules of our TDT-based receiver.

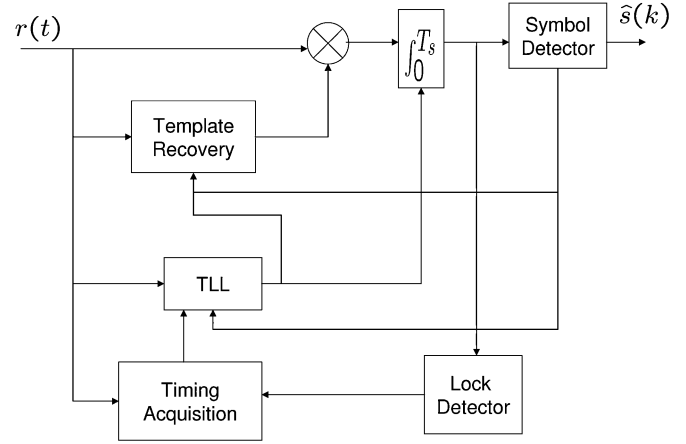


Fig. 5. Block diagram of a TDT-based receiver including a TLL.

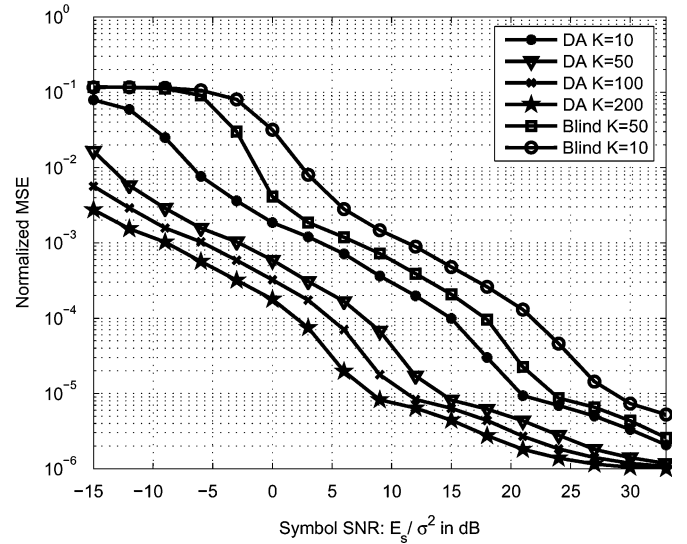


Fig. 6. Normalized MSE for blind and data-aided TDT.

## VI. SIMULATIONS

Several simulations have been performed to analyze the performance of TDT in the acquisition, demodulation, and tracking stages. The monocycle is chosen as the normalized second derivative of the Gaussian pulse  $p(t) = ((t^2 - T^2)/\sqrt{3\sqrt{\pi}T^5}/8)e^{-t^2/2T^2}$  with  $T = 1/6$  ns, having duration  $T_p = 1$  ns. Other parameters are selected as  $T_f = 35$  ns,  $N_f = 4$ , and  $B \cong 1$  GHz is the 3 dB bandwidth of the frontend lowpass filter.

### A. TDT Timing Offset Estimation Performance

In Fig. 6, the MSE of  $\hat{\tau}_0$  in data-aided and blind TDT is plotted versus symbol energy-to-noise ratio for different amounts of averaging  $K$ . The UWB channel used is model 1 as defined in [8], and the search resolution to find the maximum was set to  $T_p/10$  (0.1 ns) for both DA and non-DA TDT. The resultant detection probability is plotted versus symbol SNR in Fig. 7. Detection probability is defined as the probability that  $|\hat{\tau}_0 - \tau_0| \leq T_\Delta$ ; here  $T_\Delta$  is chosen to be 1 ns.

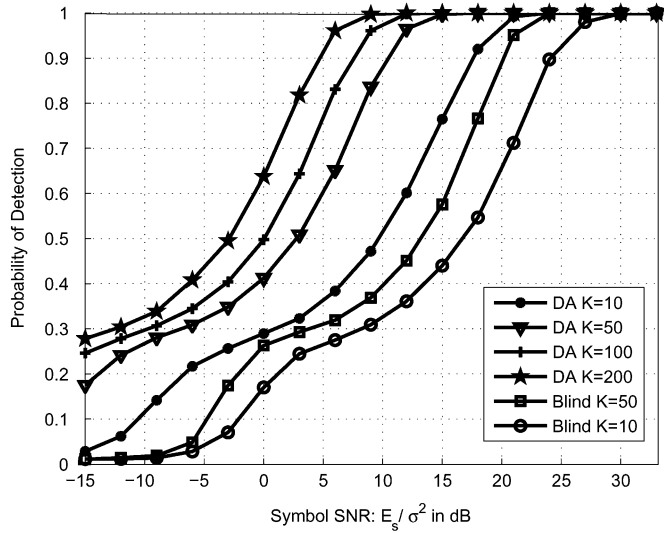


Fig. 7. Probability of detection for blind and data-aided TDT.

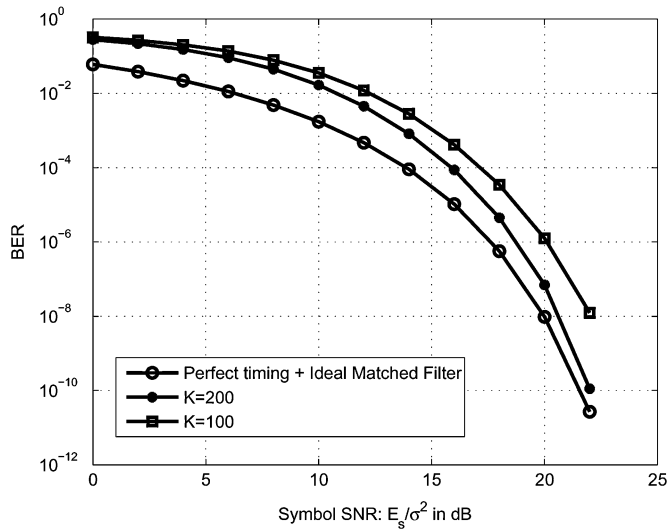


Fig. 8. BER for data-aided TDT-based demodulation with timing error 10 ns.

### B. TDT Demodulation Performance

Test A. Demodulation performance of DA-TDT in (26) when timing errors are present is illustrated in Fig. 8. Channel model 1 in [8] is used. The timing error is chosen to be  $10T_p = 10$  ns, and the BER curve corresponding to the ideal matched filter with perfect timing is also plotted as a benchmark. It can be seen that DA-TDT is very robust to mistiming and BER curves corresponding to the TDT-based demodulator in the presence of timing errors come very close to the matched filter benchmark at medium-high SNR.

Test B. Demodulation performance of TDT in terms of BER has been simulated and compared with the RAKE in Figs. 9 and 10. To highlight the dense multipath nature of the UWB channel, we use a normalized model with equally spaced taps defined as

$$\tau_l = 1.5l \text{ ns}, \quad \alpha_l = \pm \frac{1}{\sqrt{23}}, \quad \text{for } l = 0, 1, \dots, 23$$

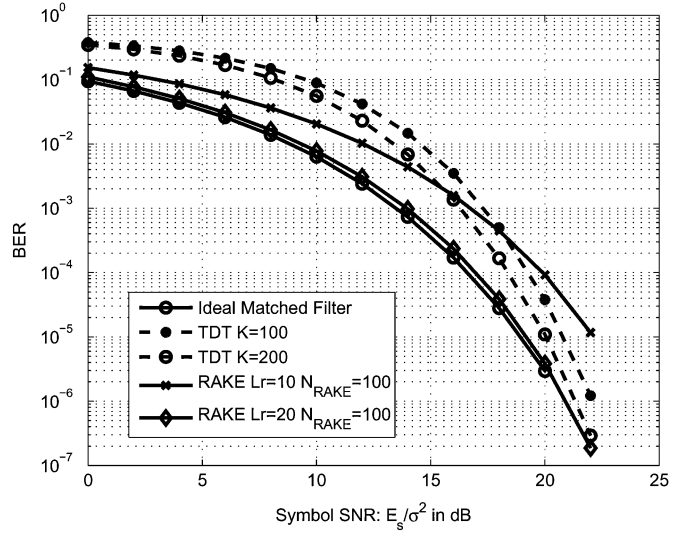
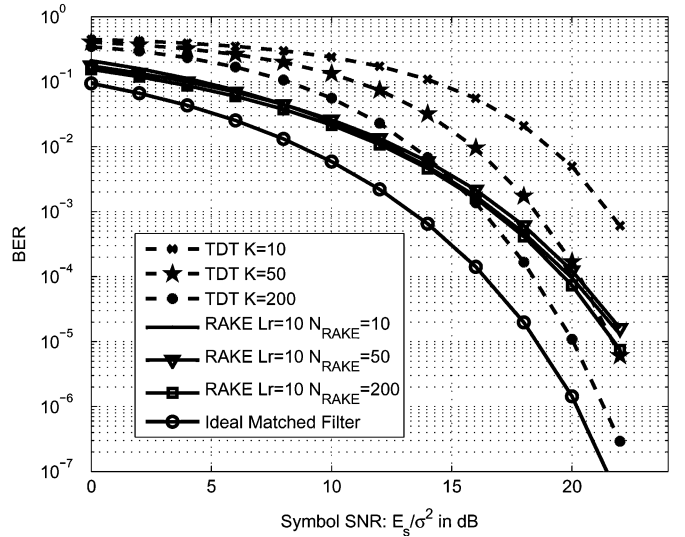


Fig. 9. BER comparison between RAKE and TDT demodulators.


 Fig. 10. BER comparison between RAKE and TDT demodulators with  $L_r = 10$  RAKE fingers.

In both figures, BER is plotted versus symbol SNR. From Fig. 9, it is clear that RAKE performs poorly when the number of fingers is small. Increasing the number of fingers may not be affordable in the UWB regime, where  $L$  can easily exceed 25. On the other hand, TDT performance can be improved by simply increasing the amount of averaging  $K$ . At high SNR, the BER curves for TDT come very close to the performance achieved through ideal matched filtering. Fig. 10 illuminates the difference between RAKE and TDT receivers. For TDT, more averaging leads to improved performance and markedly lower BER, while for RAKE increasing the length of training beyond a certain point offers no improvement. In fact, the only way to improve RAKE performance is by adding fingers which certainly demands more hardware and increases complexity. Note that the slope of TDT curves drops faster than those of RAKE.

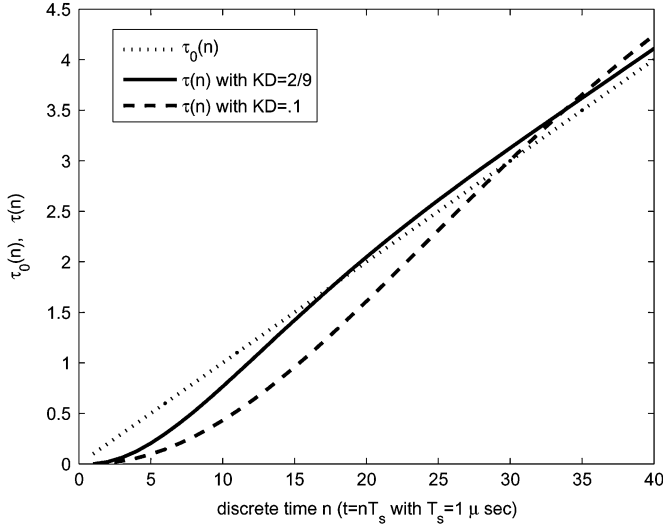


Fig. 11. Transient response and tracking capability of TLL for ramp input.

As a result, although RAKE performs better at low SNR, TDT outperforms RAKE for high enough SNR.

### C. Tracking Loop Performance

The time variation of  $\tau_0$  is modeled as  $\tau_0(t) = mt$  with slope  $m = T_p/10T_s$ . We select  $\lambda = 2 \times 10^6$ , symbol period  $T_s = 1 \mu\text{sec}$ , and input noise variance  $\text{Var}(\eta_n) = 10^{-16}$  watts/Hz. The optimum  $\omega_n$  is found to be  $\omega_n = \sqrt{2} \times 10^5$  Hz, which gives  $\omega_n T_s = \sqrt{2}/10$ . This value of  $\omega_n$  satisfies  $0.53\omega_n \ll 1/T_s$ . From the S-curve in Fig. 3,  $G$  is found for a second order derivative of the Gaussian pulse to be 0.9. Since TLL operates digitally with sampling rate  $T_s$ , we have  $\tau_0(n) = 0.1nT_p$ . For these selected parameters, the optimum  $K_D$  and  $\kappa$  values are found from (52) to be  $2/9$  and  $-0.9$ , respectively. To analyze the performance of this loop, a linear TLL model similar to (4) is simulated. The tracking capability and transient performance are illustrated in Fig. 11 for the optimum  $K_D = 2/9$  and for  $K_D = 1$ . From the figure it is seen that both loops can follow the input ramp very closely. This is due to the fact that a second order loop was chosen. However, the optimum  $K_D$  exhibits better transient performance than  $K_D = 0.1$ . Still, if we increase  $K_D$  from the optimum value we even get better transient response. The obvious tradeoff is noise power at the TLL output ( $\tau$  in Fig. 4), which is plotted in Fig. 12 for the selected parameters versus a range of values for  $K_D$ . The input noise power is set to unity in Fig. 12. At the optimum  $K_D \approx 0.2$ , the TLL reduces the input noise power by a factor 5. Decreasing  $K_D$  to  $K_D = 0.1$ , will improve noise reduction while transient performance will suffer as confirmed by Fig. 11. Our optimum  $K_D$  is chosen as a compromise between these two conflicting requirements with relative weight  $\lambda = 2 \times 10^6$ .

## VII. CONCLUSION

In this paper, acquisition performance of TDT was considered first and upper bounds on the mean square error of blind and data-aided TDT estimators were derived. The scope of TDT

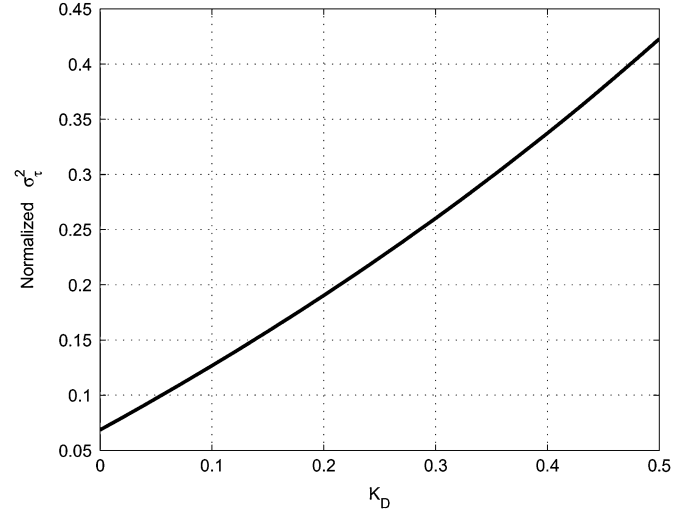


Fig. 12. TLL output noise variance versus  $K_D$  for normalized TLL input noise variance.

was broadened through TDT-based demodulation and tracking algorithms. The performance of TDT demodulators was compared with RAKE. It was shown that while RAKE suffers due to its limited number of fingers, TDT can collect full multipath energy and outperforms the RAKE at high enough SNR (15 dB in our simulations). BER and detection SNR were evaluated for TDT-based demodulators in the presence of timing errors and found to be robust to mistiming. A TDT-based TLL was also developed to account for timing offset variations due to transmitter-receiver mismatch and oscillator drifts. The tracking loop parameters were selected to jointly optimize transient and steady state TLL performance. Finally, an iterative template recovery approach was introduced to account for the slowly time varying nature of UWB channels, where templates are updated in a decision-directed fashion.<sup>1</sup>

## APPENDIX I

### PROOF OF (6)

Throughout the paper we assumed that  $\tau_0 \in [0, T_s]$ . Here we consider the case where  $\tau_0 \notin [0, T_s]$ . The proof of (6) is also detailed, to show how the sign ambiguity in  $\bar{r}(t)$  appears when  $\tau_0 \notin [0, T_s]$ . In general, we have  $\tau_0 = MT_s + \tilde{\tau}_0$ , where  $\tilde{\tau}_0 = (\tau_0)_{\text{mod } T_s} \in [0, T_s]$ . Suppose that  $M = 2q$  is even (the proof for  $M$  odd is similar). For  $t \in [0, 2T_s]$ , the template  $\bar{r}(t)$  in (3) can be written as

$$\begin{aligned} \bar{r}(t) &= \frac{1}{K} \sum_{k=0}^{K-1} (-1)^k \\ &\times \left[ \sqrt{\mathcal{E}_p} \sum_{n \text{ even}} s(n) p_R(t - nT_s - \tilde{\tau}_0 + 2kT_s - 2iT_s) \right. \\ &\left. + \eta(t + 2kT_s) \right] \end{aligned}$$

<sup>1</sup>The views and conclusions contained in this document are those of the authors and should not be interpreted as representing the official policies, either expressed or implied, of the Army Research Laboratory or the U. S. Government.

$$\begin{aligned}
 & + \sqrt{\mathcal{E}_p} \sum_{n \text{ odd}} s(n) p_R(t - nT_s - \tilde{\tau}_0 + 2kT_s - 2iT_s) \Big] \\
 & = \frac{1}{K} \sum_{k=0}^{K-1} (-1)^k \left[ \sqrt{\mathcal{E}_p} \sum_n \sum_{m=0}^1 s(2n+m) \right. \\
 & \quad \times p_R(t - (2n+m+2q-2k)T_s - \tilde{\tau}_0) \\
 & \quad \left. + \eta(t+2kT_s) \right].
 \end{aligned}$$

With further computation,  $\bar{r}(t)$  is written as

$$\begin{aligned}
 \bar{r}(t) & = \frac{\sqrt{\mathcal{E}_p}}{K} \sum_{k=0}^{K-1} (-1)^k s(2k-2q) \\
 & \quad \times p_R(t + 2(k-n-q)T_s - \tilde{\tau}_0) \\
 & \quad + \frac{1}{K} \sum_{k=0}^{K-1} (-1)^k \eta(t + 2kT_s) \\
 & \quad + \frac{\sqrt{\mathcal{E}_p}}{K} \sum_{k=0}^{K-1} \sum_{n=k-1}^k (-1)^k s(2n+1) \\
 & \quad \times p_R(t + (2(k-n-q)-1)T_s - \tilde{\tau}_0)
 \end{aligned}$$

and subsequently

$$\begin{aligned}
 \bar{r}(t) & = \sum_{k=0}^{K-1} [(-1)^{2k-q} \sqrt{\mathcal{E}_p} p_R(t - \tilde{\tau}_0) \\
 & \quad + (-1)^{2k-q} \sqrt{\mathcal{E}_p} p_R(t - T_s - \tilde{\tau}_0) \\
 & \quad + (-1)^{2k-q-1} \sqrt{\mathcal{E}_p} p_R(t + T_s - \tilde{\tau}_0)] + \bar{\eta}(t) \\
 & = (-1)^q \sqrt{\mathcal{E}_p} p_R(t - \tilde{\tau}_0) + (-1)^q \sqrt{\mathcal{E}_p} p_R(t - T_s - \tilde{\tau}_0) \\
 & \quad + (-1)^{q+1} \sqrt{\mathcal{E}_p} p_R(t + T_s - \tilde{\tau}_0) + \bar{\eta}(t), \quad t \in [0, 2T_s].
 \end{aligned} \tag{53}$$

The coefficients  $(-1)^q$  and  $(-1)^{q+1}$  produce a sign ambiguity in  $\bar{r}(t)$  which should be resolved so that the correct template is recovered for use in DA-TDT based demodulation. However, as far as acquisition performance is concerned, this sign makes no difference because it cancels out. So, without loss of generality, we can assume that  $\tau_0 \in [0, T_s]$  and  $q = 0$ ; and thus, (6) is valid.

#### APPENDIX II

##### PROOF OF (8)

The proof for  $\mathbf{E}[\zeta^2(\tau)]$  can be found in [ [23], (11) and Appendix II]. A similar one for  $\mathbf{E}[\dot{\zeta}^2(\tau)]$  is derived here. In (7),  $\zeta(\tau)$  is defined as:

$$\begin{aligned}
 \zeta(\tau) & := \int_{\tau}^{T_s+\tau} \bar{r}_s(t - T_s) \bar{\eta}(t) dt + \int_{\tau}^{T_s+\tau} \bar{r}_s(t) \bar{\eta}(t - T_s) dt \\
 & \quad + \int_{\tau}^{T_s+\tau} \bar{\eta}(t - T_s) \bar{\eta}(t) dt.
 \end{aligned} \tag{54}$$

Differentiating  $\zeta(\tau)$  in (54) with respect to  $\tau$  yields:

$$\begin{aligned}
 \dot{\zeta}(\tau) & = \bar{r}_s(\tau) \bar{\eta}(\tau + T_s) - \bar{r}_s(\tau - T_s) \bar{\eta}(\tau) \\
 & \quad + \bar{r}_s(\tau + T_s) \bar{\eta}(\tau) - \bar{r}_s(\tau) \bar{\eta}(\tau - T_s) \\
 & \quad + \bar{\eta}(\tau + T_s) \bar{\eta}(\tau) - \bar{\eta}(\tau - T_s) \bar{\eta}(\tau).
 \end{aligned} \tag{55}$$

After squaring (55) and taking expected values, the following terms remain:

$$\begin{aligned}
 \mathbf{E}[\dot{\zeta}^2(\tau)] & = \bar{r}_s^2(\tau) \mathbf{E}[\bar{\eta}^2(\tau + T_s)] + \bar{r}_s^2(\tau - T_s) \mathbf{E}[\bar{\eta}^2(\tau)] \\
 & \quad - \bar{r}_s(\tau - T_s) \bar{r}_s(\tau + T_s) \mathbf{E}[\bar{\eta}^2(\tau)] \\
 & \quad + \bar{r}_s^2(\tau + T_s) \mathbf{E}[\bar{\eta}^2(\tau)] + \bar{r}_s^2(\tau) \mathbf{E}[\bar{\eta}^2(\tau - T_s)] \\
 & \quad + \mathbf{E}[\bar{\eta}^2(\tau)] \mathbf{E}[\bar{\eta}^2(\tau + T_s)] + \mathbf{E}[\bar{\eta}^2(\tau)] \mathbf{E}[\bar{\eta}^2(\tau - T_s)]
 \end{aligned} \tag{56}$$

where we used that  $\mathbf{E}[\bar{\eta}(\tau - T_s) \bar{\eta}(\tau)] = \mathbf{E}[\bar{\eta}(\tau + T_s) \bar{\eta}(\tau)] = \mathbf{E}[\bar{\eta}(\tau - T_s) \bar{\eta}(\tau + T_s)] = 0$ . These expressions hold, since  $T_s \gg T_p \approx 1/B$ . Using the two facts:  $\bar{r}_s^2(\tau - T_s) = \bar{r}_s^2(\tau) = \bar{r}_s^2(\tau + T_s)$ , and  $\mathbf{E}[\bar{\eta}^2(t)] = B\sigma^2/K$ , we can simplify (56) to

$$\mathbf{E}[\dot{\zeta}^2(\tau)] = 3 \left( \frac{B\sigma^2}{K} \right) \bar{r}_s^2(\tau) + 2 \left( \frac{B\sigma^2}{K} \right)^2. \tag{57}$$

However,  $\bar{r}_s(\tau_0) = 0$  from (6). Using this fact in (57) we arrive at the desired result for  $\mathbf{E}[\dot{\zeta}^2(\tau_0)]$ . The expression for  $\mathbf{E}[\zeta(\tau) \dot{\zeta}(\tau)]$  follows along similar steps.

#### APPENDIX III

##### PROOF OF (18)

We wish to evaluate  $\mathbf{E}[J_{\text{DA}}^2(\tau_0)]$ . From (7),  $J_{\text{DA}}^2(\tau)$  can be written as

$$\begin{aligned}
 J_{\text{DA}}^2(\tau)|_{\tau=\tau_0} & = 4\chi^2 \dot{\chi}^2 + 4\chi^2 \dot{\zeta}^2 + 4\chi^2 \zeta^2 + 16\chi \dot{\chi} \zeta \dot{\zeta} \\
 & \quad + \text{S.N.T.} + \text{H.O.P.}
 \end{aligned} \tag{58}$$

where the  $\tau$ -dependence of terms in (58) is dropped, for brevity; S.N.T. denotes single noise terms and H.O.P. denotes higher order perturbations, meaning terms containing three or four noise factors. Considering expected values of both sides of (58) and using  $\dot{\chi}(\tau_0) = 0$ , we arrive at

$$\mathbf{E}[J_{\text{DA}}^2(\tau_0)] = 4\chi^2(\tau_0) \mathbf{E}[\dot{\zeta}^2(\tau_0)].$$

Substituting for  $\chi(\tau_0)$  and  $\mathbf{E}[\dot{\zeta}^2(\tau_0)]$  from (11) and (8) completes the proof of (18).

#### REFERENCES

- [1] C. Carbonelli, U. Mengali, and U. Mitra, "Synchronization and channel estimation for UWB signals," in *Proc. GLOBECOM Conf.*, vol. 2, San Francisco, CA, Dec. 1–5, 2003, pp. 764–768.
- [2] C. C. Chui and R. A. Scoltz, "Tracking UWB monocycles in IEEE 802.15 multipath channels," in *Proc. 37th Asilomar Conference Signals, Systems and Computers*, vol. 2, Pacific Grove, CA, Nov. 2003, pp. 1761–1765.
- [3] M.-H. Chung and R. A. Scholtz, "Comparison of transmitted-and stored-reference systems for ultra-wideband communications," in *Proc. MIL-COM Conf.*, Monterey, CA, Oct. 31–Nov. 3 2004.

- [4] F. M. Gardner, "Demodulator Reference Recovery Techniques Suited for Digital Implementation," *European Space Agency Final Report ESTEC Contract No. 6847/86/NL/DG*, Aug. 1988.
- [5] R. Hoocher and H. Tomlinson, "Delay-hopped transmitted-reference RF communication," in *Proc. Conf. Ultra Wideband Systems and Technologies*, Baltimore, MD, May 2002, pp. 265–269.
- [6] RCD Components Inc. [Online]. Available: <http://216.153.156.169:8080/rcd/rcdpdf/P1410-P2420.pdf>.
- [7] J. P. Ianniello, "Large and small error performance limits for multipath time delay estimation," *IEEE Trans. Acoust., Speech, Signal Process.*, vol. 34, no. 2, pp. 245–251, Apr. 1986.
- [8] "Channel Modeling Sub-Committee Report Final," IEEE P802.15 Working Group for WPANs, IEEE P802.15-02/368r5-SG3a, Nov. 2002.
- [9] R. Jaffe and E. Rehtin, "Design and performance of phase-lock circuits capable of near-optimum performance over a wide range of input signal and noise levels," *IRE Trans. Inf. Theory*, vol. 1, pp. 66–76, Mar. 1955.
- [10] W. C. Lindsey and C. M. Chie, "A survey of digital phase-locked loops," *Proc. IEEE*, vol. 69, no. 4, pp. 410–431, Apr. 1981.
- [11] V. Lottici, A. D. Andrea, and U. Mengali, "Channel estimation for ultra-wideband communications," *IEEE J. Sel. Areas Commun.*, vol. 20, pp. 1638–1645, Dec. 2002.
- [12] X. Luo and G. B. Giannakis, "Low complexity blind synchronization and demodulation for (ultra-) wideband multi-user *ad hoc* access," *IEEE Trans. Wireless Commun.*, 2005. (to appear) [Online]. Available <http://www.ece.umn.edu/users/xluo/research.htm>
- [13] —, "Cyclic-mean based synchronization and efficient demodulation for UWB *ad hoc* access: generalizations and comparisons," *EURASIP: Signal Processing Journal*, 2005, to be published.
- [14] U. Mengali and A. N. D'Andrea, *Synchronization Techniques for Digital Receivers* ch. 7. New York: Plenum, 1997.
- [15] H. Meyr and G. Ascheid, *Synchronization in Digital Communications*, vol. 1, 1st ed., New York: Wiley, 1990, ch. 2–3.
- [16] H. Niu, J. A. Ritcey, and H. Liu, "Performance of UWB RAKE receivers with imperfect tap weights," in *Proc. Int. Conf. on ASSP*, vol. 4, Hong Kong, China, Apr. 4–6, 2003, pp. 125–128.
- [17] H. Sheng, R. You, and A. M. Haimovich, "Performance analysis of ultra-wideband RAKE receivers with channel delay estimation errors," in *Proc. 38th Conf. Info. Sciences and Systems*, Princeton, NJ, Mar. 2004, pp. 921–926.
- [18] Z. Tian and G. B. Giannakis, "A GLRT approach to data-aided timing acquisition in UWB radios—Part I: algorithms," *IEEE Trans. Wireless Commun.*, 2005 (to appear).
- [19] Z. Wang and X. Yang, "Ultra wide-band communications with blind channel estimation based on first-order statistics," in *Proc. ICASSP Conf.*, Montreal, Quebec, Canada, May 2004, pp. 529–532.
- [20] M. Z. Win and R. A. Sclott, "Ultra wide bandwidth time-hopping spread-spectrum impulse radio for wireless multiple access communications," *IEEE Trans. Commun.*, vol. 48, no. 4, pp. 679–691, Apr. 2000.
- [21] L. Wu, X. Wu, and Z. Tian, "RAKE versus noisy template based UWB receivers under timing and channel estimation errors," in *Proc. Int. Conf. Communications*, Seoul, Korea, May 2005.
- [22] L. Yang and G. B. Giannakis, "Ultra-wideband communications: an idea whose time has come," *IEEE Signal Process. Mag.*, vol. 21, no. 6, pp. 26–54, Nov. 2004.
- [23] —, "Timing UWB signals using dirty template," *IEEE Trans. Commun.*, 2005 (to appear) [Online]. Available <http://spincom.ece.umn.edu/>
- [24] —, "Optimal pilot waveform assisted modulation for ultrawideband commun.," *IEEE Trans. Wireless Commun.*, vol. 3, no. 4, pp. 1236–1249, Jul. 2004.
- [25] H. Zhang and D. L. Goeckel, "Generalized transmitted-reference UWB systems," in *Proc. Conf. Ultra Wideband Systems and Technologies*, Reston, VA, Nov. 2003, pp. 147–151.



**Shahrokh Farahmand** received the B.S. degree in electrical engineering from Sharif University of Technology, Tehran, Iran in 2003. Since then, he has been working toward the Ph.D. degree at the Department of Electrical and Computer Engineering, University of Minnesota, Twin Cities.

His research interests include the areas of signal processing, communication theory, and networking. His current research focuses on ultra-wide band wireless communications.



**Xiliang Luo** (S'03) received the B.S. degree in physics from the Peking University, Beijing, China, in 2001, and the M.Sc. degree in electrical engineering from the University of Minnesota, in 2003. He is currently a Ph.D. candidate in the Department of Electrical and Computer Engineering at the University of Minnesota.

His general research interests lie in signal processing, communications, and information theory. Currently, he is focusing on ultra wideband (UWB) communications and wireless sensor networks (WSN).



**Georgios B. Giannakis** (F'97) received the Diploma in Electrical Engineering from the National Technical University of Athens, Greece, 1981. From September, 1982 to July, 1986, he was with the University of Southern California (USC), where he received the M.Sc. in electrical engineering in 1983, M.Sc. in mathematics in 1986, and Ph.D. in electrical engineering in 1986.

After lecturing for one year at USC, he joined the University of Virginia in 1987, where he became a Professor of Electrical Engineering in 1997. Since 1999 he has been a Professor with the Department of Electrical and Computer Engineering at the University of Minnesota, where he now holds an ADC Chair in Wireless Telecommunications. His general interests span the areas of communications and signal processing, estimation and detection theory, time-series analysis, and system identification—subjects on which he has published more than 220 journal papers, 380 conference papers, and two edited books. Current research focuses on transmitter and receiver diversity techniques for single- and multiuser fading communication channels, complex-field and space-time coding, multicarrier, ultrawide band wireless communication systems, cross-layer designs and sensor networks.

Dr. Giannakis is the corecipient of six paper awards from the IEEE Signal Processing (SP) and Communications Societies (1992, 1998, 2000, 2001, 2003, 2004). He also received the SP Society's Technical Achievement Award in 2000. He served as Editor in Chief for the *IEEE SP Letters*, as Associate Editor for the *IEEE Transactions on Signal Processing* and the *IEEE SP Letters*, as Secretary of the SP Conference Board, as Member of the SP Publications Board, as Member and Vice-Chair of the Statistical Signal and Array Processing Technical Committee, as Chair of the SP for Communications Technical Committee, and as a Member of the IEEE Fellows Election Committee. He has also served as a member of the IEEE-SP Society's Board of Governors, the Editorial Board for the *Proceedings of the IEEE*, and the steering committee of the *IEEE Transactions on Wireless Communications*.